Analysis of Cooperative Conformational Transitions in Cellulose and Amylose Tricarbanilates

Benjamin Hsu, Charles A. McWherter, and David A. Brant*

Department of Chemistry, University of California, Irvine, California 92717

Walther Burchard

Institut für Makromolekulare Chemie, Universität Freiburg, D-7800 Freiburg i.Br., West Germany. *Received December 29, 1981*

ABSTRACT: Dissolved cellulose tricarbanilate (CTC) and amylose tricarbanilate (ATC) both exhibit temperature- and solvent-induced transitions between forms of differing stiffness and chain extension. The transition temperatures are strongly dependent on chain length, suggesting that the transitions are very cooperative (Gupta, A. K.; Marchal, E.; Burchard, W.; Pfannemueller, B. *Macromolecules* **1979**, *12*, 281). It is shown in this paper that the chain length dependences of the unperturbed dimensions of CTC and ATC (Burchard, W. *Br. Polym. J.* **1971**, *3*, 214) also reflect the cooperative conformational transitions inferred from other kinds of measurements. The method of Miller and Flory (Miller, W. G.; Flory, P. J. *J. Mol. Biol.* **1966**, *15*, 298) and realistic chain models for the two polymers are used to fit the observed chain length dependences of the unperturbed dimensions. Zimm–Bragg cooperativity parameters σ on the order of 10^{-5} and 10^{-6} for CTC and ATC, respectively, are required to match the slow convergence of the characteristic ratios to their asymptotic values at high degrees of polymerization. We have been unable to fit the data in question with any model that does not involve a *cooperative* transition from a more flexible form of the chain skeleton, which predominates at low degrees of polymerization, to a less flexible form, the stability of which is enhanced at high degrees of polymerization. The theoretical models providing the best fits to the unperturbed dimension data are used to calculate persistence lengths of 110 and 103 Å for CTC and ATC, respectively. The models are also used to demonstrate, in terms of the calculated directional correlation function of the terminal bonds of the chain, that directional correlations persist over a substantially larger number of residues in ATC than in CTC.

Introduction

The tricarbanilate derivatives of cellulose (CTC) and amylose (ATC) exhibit conformational transitions in solution, induced either by changes in temperature in a given solvent or by changes in mixed-solvent composition at fixed temperature. More extended and less flexible forms of the polymers occur in the ether solvent dioxane, whereas in ester and ketone solvents such as acetone, ethyl acetate, and phenyl benzoate the polymers adopt more flexible conformations.[1-8] Evidence for the temperature- and solvent-induced conformational changes is perhaps clearest in measurements of light scattering,[1] flow birefringence,[5] intrinsic viscosity,[5] and critical dielectric frequency.[4,8] Variations in temperature produce sigmoidal transition curves for the critical dielectric frequency of CTC[4] and ATC[8] in dioxane solution, where both polymers manifest extended and relatively inflexible forms at low temperature.[1,4-8] The very pronounced molecular weight dependence of the latter curves suggests that the temperature-induced transition in question is quite cooperative, at least in dioxane.[4,8]

Considerable information exists concerning the conformations of CTC and ATC in dioxane solution, and the temperature and chain length dependences of various parameters characterizing the conformation, e.g., radius of gyration,[2] intrinsic viscosity,[5,7] persistence length,[4-6,8] and persistence dipole moment,[4,8] have been observed. Moreover, a careful determination of the unperturbed mean-square radius of gyration $\langle s_x^2 \rangle_0$ of CTC and ATC in the well-behaved[1,2] mixed Θ solvent dioxane/methanol has been carried out at 20 °C over an unusually wide range of degree of polymerization x;[3] samples with degrees of polymerization in the range $84 \leq x \leq 6930$ for CTC and in the range $86 \leq x \leq 9400$ for ATC were investigated. The chain length dependence of the characteristic parameter $\langle s_x^2 \rangle_0 / x$, corrected for molecular weight heterogeneity in the polymer samples, has been analyzed earlier in terms of various chain models by one of us.[3] Here, we reanalyze these data using the statistical mechanical theory of polymer chain configuration and more realistic theoretical models for the CTC and ATC chains. In addition, in the present treatment we take cognizance of the significant effect on the chain length dependence of $\langle s_x^2 \rangle_0 / x$ to be expected from the putative highly cooperative conformational transition inferred from other recent studies.[4,8]

Theoretical Methods

Chain Models for CTC and ATC. The skeletal geometries of the CTC and ATC repeating units were taken to be those, respectively, of the averaged β-D-glucose and α-D-glucose residues proposed by Arnott and Scott;[9] other approximations in the models render negligible differences between the geometries of the unsubstituted α- and β-D-glucose and those of the phenylcarbamate-substituted residues. The valence angle β at the oxygen of the glycosidic bridge between successive residues was taken to be 116.5°.[9] The pyranoside ring of each substituted sugar residue was assumed to be rigid so as to render the "virtual bond" distance L between successive glycosidic oxygens fixed at the values 5.47 and 4.40 Å, respectively, for the CTC and ATC chains.[9] With this approximation, which is common to most analyses of the configurational statistics of the polysaccharides, the chains can be understood to comprise a sequence of virtual bonds of constant length, the mutual orientations of any two of which are governed by the torsion angles ϕ and ψ about the C(1)–O(1) and O(1)–C(4′) bonds, respectively, of the intervening glycosidic linkages.[10]

In contrast to most other treatments of polysaccharide chain statistics, we will not assume here that the glycosidic torsions ϕ_i,ψ_i at the linkage joining residues i and $i+1$ are independent of the conformations of neighboring glycosidic linkages.[11] In the present case we wish instead to acknowledge the possibility of longer range cooperative interactions within the chain that could cause the potential function governing rotations ϕ_i,ψ_i to depend upon the conformational state of neighboring residues. To this end we will assume that each residue i is capable of existing

0024-9297/82/2215-1350$01.25/0

in two states, in each of which the conformational potential function for the associated rotations ϕ_i,ψ_i adopts a characteristic form. Specifically, the potential function for the "flexible" state will allow ϕ_i,ψ_i to adopt a range of conformations, which if available to a succession of residues would yield a relatively flexible polymer chain segment. The potential function governing the "stiff" state would, in contrast, constrain more closely the accessible range of conformation space so that a sequence of residues all in the stiff state would constitute a relatively less flexible chain segment.

The origin of differences between the flexible and stiff conformational potential functions is assumed to reside in the existence of long-range interactions, characteristic of the stiff state of the chain, that restrict the conformational freedom of ϕ_i,ψ_i pairs contained within such stiff regions of the chain. The physical basis of such long-range interactions might be, for example, solvophobic and/or hydrogen-bonded interactions between the phenylcarbamate substituent groups.[4,8] The distribution of residues between the two postulated states is assumed in the present treatment to be governed by parameters s and σ of the Zimm–Bragg type,[12] where s describes the relative stability of residues embedded in long sequences of each state and σ measures the extra free energy associated with the interface between sequences of residues in contrasting states.[13] The quantity s will be treated as an adjustable parameter of the calculation, but realistic values will for present purposes necessarily be confined to $s \simeq 1$, because the temperature-induced transition is observable in the vicinity of room temperature.[4,8] The parameter σ is intimately related to the chain length dependence of the temperature-induced transition and can consequently be estimated[14,15] from the observed chain length dependence of the thermal transition in the critical dielectric frequency.[4,8]

For a residue i in either one of the postulated states it will be assumed that the conformational characteristics of the residue depend on a potential function that varies only with ϕ_i,ψ_i. Interdependence of rotations ϕ_i,ψ_i with neighboring rotations exists in this treatment then in the sense that the probability (as governed by s and σ) that a given residue is in a particular state is dependent, in the presence of the postulated cooperative interactions, on the states of the neighboring residues. Thus, the torsions at a given glycosidic linkage, while mutually interdependent, are assumed independent of all other such sets of torsions for any given permutation of the residues of the chain among the stiff and flexible states.[10]

Conformational Energies. Conformational energies $V_c(\phi_i,\psi_i)$ for the glycosidic linkages of CTC and ATC will be approximated by parabolic or harmonic surfaces centered at positions in the ϕ_i,ψ_i plane known to be appropriate from more realistic estimates of the conformational energy surfaces of cellulosic and amylosic chains.[16–18] Equation 1 gives $V_c(\phi_i,\psi_i)$. Here, the subscript c designates

$$V_c(\phi_i,\psi_i) = \frac{K_c^{\phi}}{2}(\phi_i - \phi_0)^2 + \frac{K_c^{\psi}}{2}(\psi_i - \psi_0)^2 \qquad (1)$$

either the flexible (f) or the stiff (s) conformational state. The minimum energy (zero) occurs at the position ϕ_0,ψ_0 selected as described below. Adjustable parameters K_c^{ϕ} and K_c^{ψ} govern the steepness of the potential walls and, thus, the size of the accessible domain in conformation space; larger values of K_c^{ϕ} and K_c^{ψ} correspond to the less flexible conformational states. In all calculations reported here surfaces of circular cross section ($K_c^{\phi} = K_c^{\psi}$) were chosen, because no sensible improvement in the treatment was realized when surfaces of elliptical cross section ($K_c^{\phi} \neq K_c^{\psi}$) were taken. When $K_c^{\phi} = K_c^{\psi}$ is not too small, the potential surfaces of eq 1 correspond to polymer chains of wormlike character.[18,19] Results reported below suggest that attempts to use more realistic potential surfaces appropriate to the specific geometries of the tricarbanilate derivatives will, at this stage, convey no additional insights into the behavior of these chains.

Methods of Calculation. The property of primary interest in the present study is the dependence on chain length x of the unperturbed mean-square radius of gyration $\langle s_x^2\rangle_0$ from light scattering; fits to existing data[3] are reported. The best models achieved for CTC and ATC are then used to calculate the persistence length a_x,[18–20] the end-bond correlation function f_x,[18,20,21] and the fraction of residues in the stiff state $\theta_{s,x}$[22,23] as functions of chain length. The methods used are essentially those of Miller and Flory.[22,23]

Let $\mathbf{M}_i$ be an appropriately constructed generator matrix associated with the property m to be calculated. Then the statistical mechanical average $\langle m_x\rangle$ for chains of length x is given by

$$\langle m_x\rangle = Z_x^{-1}\mathbf{m}_1\mathbf{m}_2...\mathbf{m}_i...\mathbf{m}_x \qquad (2)$$

where one factor $\mathbf{m}_i$ appears in the serial matrix product for each residue of the chain.[24] Here, $\mathbf{m}_i$ is defined for $1 < i < x$ by

$$\mathbf{m}_i = \begin{bmatrix} s\mathrm{M}_i(\mathrm{s}) & \mathrm{M}_i(\mathrm{f}) \\ \sigma s\mathrm{M}_i(\mathrm{s}) & \mathrm{M}_i(\mathrm{f}) \end{bmatrix} \qquad (3)$$

with $\mathbf{m}_1$ = row $[\sigma s\mathbf{M}_1(\mathrm{s}),\mathbf{M}_1(\mathrm{f})]$ and $\mathbf{m}_x$ = col $[\mathbf{M}_x,\mathbf{M}_x]$. The notation $\mathbf{M}_i(\mathrm{c})$, where c is either s or f, denotes matrices $\mathbf{M}_i$ appropriate for the stiff and flexible states, respectively; matrix $\mathbf{M}_x$ is independent of the conformational state of the residue. The quantity Z_x in eq 2 is the partition function calculated by

$$Z_x = \mathbf{U}_1\mathbf{U}_2...\mathbf{U}_i...\mathbf{U}_x \qquad (4)$$

where for $1 < i < x$

$$\mathbf{U}_i = \begin{bmatrix} s & 1 \\ \sigma s & 1 \end{bmatrix} \qquad (5)$$

with $\mathbf{U}_1$ = row $[\sigma s,1]$ and $\mathbf{U}_x$ = col $[1,1]$.

It is implicit in the above equations that the parameter s measures the statistical weight of a residue in the stiff state relative to the weight unity in the flexible state. The fraction $\theta_{s,x}$ of residues in the stiff state then follows immediately by differentiation of $\ln Z_x$ with respect to $\ln s$,[12] an operation accomplished in the present instance by using the matrix method described by Miller and Flory.[22]

If we let $\mathbf{L}_i$ represent the virtual bond vector of residue i referred to a coordinate system affixed to residue i and take $\hat{\mathbf{T}}_i(\phi_i,\psi_i)$ to be the 3×3 orthogonal matrix that transforms vectors referred to the coordinate system of residue $i+1$ into the coordinate system of residue i,[10,25] then the generator matrix $\mathbf{A}_i(\mathrm{c})$ of generic type $\mathbf{M}_i(\mathrm{c})$ needed to compute the mean end-to-end vector $\langle\mathbf{r}_x\rangle$ of the polymer is given for $1 < i < x$ by[19,24]

$$\mathbf{A}_i(\mathrm{c}) = \begin{bmatrix} \langle\hat{\mathrm{T}}_i\rangle & \mathrm{L}_i \\ \mathbf{0} & 1 \end{bmatrix} \qquad (6)$$

with $\mathbf{A}_1(\mathrm{c})$ = row $[\langle\hat{\mathbf{T}}_1\rangle,\mathbf{L}_1]$ and $\mathbf{A}_x$ = col $[\mathbf{L}_x,1]$. Here $\mathbf{0}$ represents the 1×3 null vector, so that $\mathbf{A}_i(\mathrm{c})$ has dimensions 4×4 while $\mathbf{A}_1(\mathrm{c})$ and $\mathbf{A}_x$ have dimensions 3×4 and

4 × 1, respectively. The quantity $\langle \hat{\mathbf{T}}_i \rangle$ is the transformation matrix $\hat{\mathbf{T}}_i(\phi_i,\psi_i)$ averaged[10,25] over the conformational energy surface appropriate to residue i in the stiff or the flexible state, as required by the index c. Under the assumptions of the present model the homopolymer residue geometry is fixed, so that for all i, $\mathbf{L}_i = \mathbf{L}$ and $\hat{\mathbf{T}}_i(\phi_i,\psi_i) = \hat{\mathbf{T}}$. The persistence length a_x reported here is the magnitude of $\langle \mathbf{r}_x \rangle$ for chains of x residues.[18-20]

We define the end-bond correlation function f_x as the mean projection of a unit vector along $\mathbf{L}_x$ onto the direction of $\mathbf{L}_1$.[18,20,21] It can be computed by using the generator matrix $\mathbf{F}_i(c)$ defined for $1 < i < x$ by $\mathbf{F}_i(c) = \langle \hat{\mathbf{T}}_i \rangle$ with $\mathbf{F}_1(c) = \mathbf{u}_1\langle \hat{\mathbf{T}}_1 \rangle$ and $\mathbf{F}_x = \mathbf{u}_x$, where $\mathbf{u}_1 = \mathbf{u}_x = \mathbf{L}/|\mathbf{L}|$. The unperturbed mean-square radius of gyration $\langle s_x^2 \rangle_0$ is calculated by using the generator matrix $\mathbf{H}_i$ given by[26]

$$\mathbf{H}_i(c) = \begin{bmatrix} 1 & 1 & 2\mathbf{L}_i\langle \mathbf{T}_i \rangle & L_i^2 & L_i^2 \\ 0 & 1 & 2\mathbf{L}_i\langle \mathbf{T}_i \rangle & L_i^2 & L_i^2 \\ \mathbf{0} & \mathbf{0} & \langle \mathbf{T}_i \rangle & \mathbf{L}_i & \mathbf{L}_i \\ 0 & 0 & 0 & 1 & 1 \\ 0 & 0 & \mathbf{0} & 0 & 1 \end{bmatrix} \quad (7)$$

with $\mathbf{H}_1(c)$ = row $[1,1,2\mathbf{L}_1\langle \hat{\mathbf{T}}_1 \rangle, L_1^2, L_1^2]$ and $\mathbf{H}_x(c)$ = col $[L_x^2, L_x^2, \mathbf{L}_x, 1, 1]$. The dimensions of $\mathbf{H}_i(c)$ are 7 × 7 for $1 < i < x$ and 1 × 7 and 7 × 1 for $\mathbf{H}_1(c)$ and $\mathbf{H}_x(c)$, respectively. The quantity $\mathbf{0}$ is a 1 × 3 or 3 × 1 null vector as required to conform, and L_i is the magnitude of $\mathbf{L}_i$. Theoretical and experimental results pertaining to $\langle s_x^2 \rangle_0$ are reported here in terms of the dimensionless characteristic ratio[10] $\langle s_x^2 \rangle_0/xL^2$, where L is the magnitude of $\mathbf{L}$.

Results and Discussion

Evaluation of σ. The parameter σ was estimated via methods proposed by Fujita and co-workers[14,15] from the chain length dependence of the temperature-induced transition in the critical dielectric frequencies of CTC[4] and ATC[8] in dioxane. Data covering the ranges $250 \leq x \leq 742$ and $40 \leq T \leq 70$ °C for CTC and the ranges $125 \leq x \leq 560$ and $50 \leq T \leq 70$ °C for ATC were used. Neither the method of Hayashi et al.[14] nor that of Okita et al.[15] proved entirely satisfactory. In the case of the method of Okita et al. the condition $x\sigma^{1/2} > 2$ was not met for all polymer samples, and the required plots of $\theta_{s,x}$ vs. $(x-2)^{-1}$ at a given temperature, expected to be linear, were not always so. The iterative procedure of Hayashi et al. did not converge as well as might have been hoped. Nevertheless, using the two methods it was possible to determine $\sigma = 1.1 \times 10^{-5}$ for CTC and $\sigma = 3.0 \times 10^{-5}$ for ATC. In each case the uncertainty attributable to σ is at least a factor of 2, and we have consequently felt free to adjust σ modestly to improve fits to data on $\langle s_x^2 \rangle_0$ vs. x in the dioxane/methanol Θ solvent at 20 °C.

Chain Length Dependence of $\langle s_x^2 \rangle_0/xL^2$ for CTC. A contour diagram of the conformational energy surface for a dimeric segment of an unsubstituted cellulosic chain is shown in Figure 1. This surface was calculated as described elsewhere.[16-18] The energetically accessible domain in conformation space is seen to occur near the position $\phi_i,\psi_i = 0,0°$. Preliminary efforts to fit experimental results on the chain length dependence of the characteristic ratio $\langle s_x^2 \rangle_0/xL^2$ were therefore based on parabolic energy surfaces centered at the position $\phi_0,\psi_0 = 0,0°$. Letting K_s^ϕ, K_s^ψ, K_f^ϕ, and K_f^ψ be identical and successively equal to 2, 3, 4, and 5 kcal/mol with $\phi_0,\psi_0 = 0,0°$, one obtains the curves for $\langle s_x^2 \rangle_0/xL^2$ shown in Figure 2. These calculations correspond to choosing the stiff and flexible states to be indistinguishable, and consequently the results are independent of σ and s. Similar calculations are referred to henceforth as "one-state" models. Energies

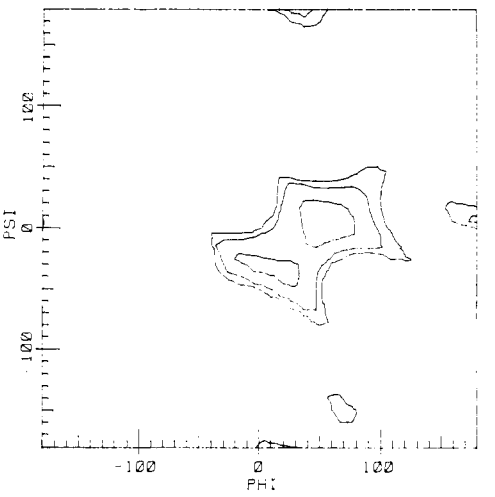

Figure 1. Contour diagram of the conformational energy of the dimeric cellulosic chain segment, cellobiose, based on Arnott–Scott[9] residue geometry, a glycosidic bridge angle of 116.5°, and potential functions described previously.[11,16] Energy contours are drawn at 1, 5, and 10 kcal/mol above the energy minimum.

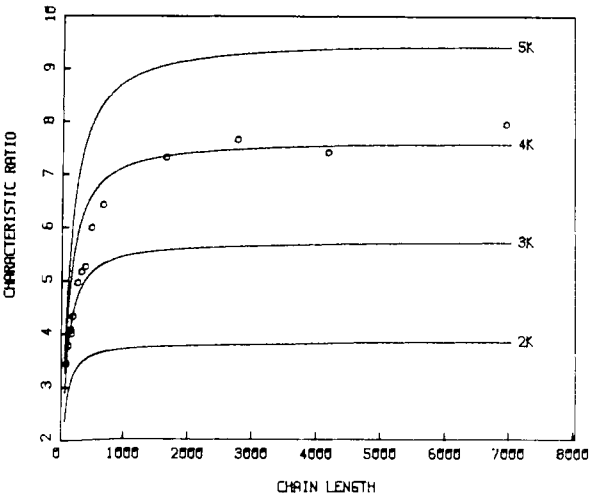

Figure 2. Circles represent experimental results[3] for the characteristic ratio $\langle s_x^2 \rangle_0/xL^2$ as a function of degree of polymerization x for CTC. Curves are calculated from a one-state model with various parabolic potential surfaces as described in the text.

were computed via eq 1, with angles measured in radians. Averages over these parabolic energy surfaces were computed by summations on a grid at 20° intervals in ϕ,ψ space.[10]

The small circles plotted in Figure 2 are the experimental values of $\langle s_x^2 \rangle_0/xL^2$ observed for CTC in the dioxane/methanol Θ solvent at 20 °C.[3] These and all other one-state models, including those with presumably more realistic energy surfaces, e.g., Figure 1, failed to provide an adequate fit to the experimental results. Models yielding chains sufficiently extended to fit the asymptotic values of the characteristic ratio at high degrees of polymerization, e.g., the 4K model in Figure 2, overestimated the ratio at lower degrees of polymerization. On the other hand, models such as the 3K model in Figure 2, which fit the data at low degrees of polymerization, yield $\langle s_x^2 \rangle_0/xL^2$ values significantly below the experimental asymptotic limit. The implication that the real chain grows stiffer with increasing chain length is obvious.

Calculations based on the "two-state" model are presented in Figure 3. The curve labeled 6K3K refers, for example, to a calculation in which the potential function for the stiff state is characterized by $K_s^\phi = K_s^\psi = K_s = 6$

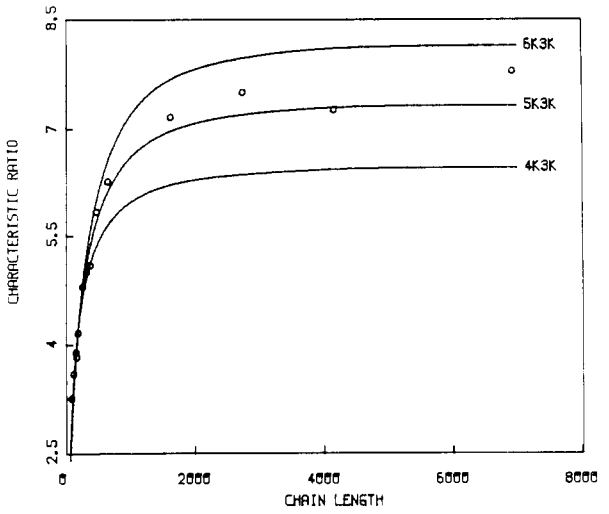

Figure 3. Calculated dependence of $\langle s_x^2\rangle_0/xL^2$ on x for CTC using a two-state model with various potential surfaces for the stiff state.

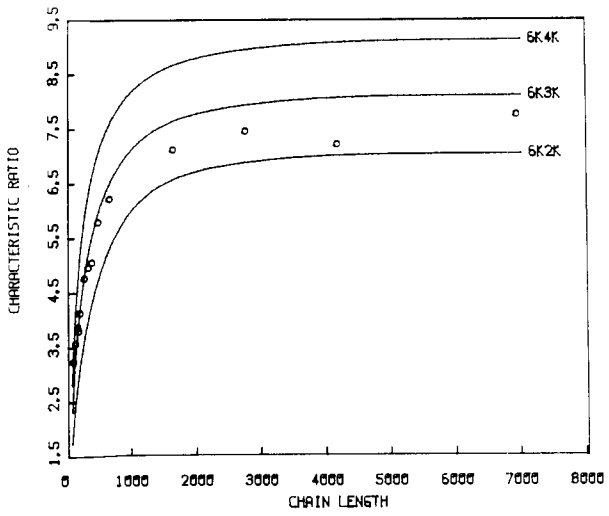

Figure 4. Calculated dependence of $\langle s_x^2\rangle_0/xL^2$ on x for CTC using a two-state model with various potential surfaces for the flexible state.

kcal/mol and that for the flexible state by $K_f^{\phi} = K_f^{\psi} = K_f$ = 3 kcal/mol. For these calculations s = 1.00 and $\sigma = 1.1 \times 10^{-5}$, with ϕ_0,ψ_0 = 0,0° for both the stiff and the flexible states. Since s = 1.00, at large x, $\theta_{s,x}$ approaches 0.5, whereas at small x, $\theta_{s,x}$ approaches zero, and residues in the flexible state predominate. Hence the three curves in Figure 3 merge at low x because they share common values of K_f. The 5K3K model provides an improved fit to the experimental data compared with the one-state models. Figure 4 illustrates the effect of variations in K_f when K_s is held constant for s = 1.00, $\sigma = 1.1 \times 10^{-5}$, and ϕ_0,ψ_0 = 0,0° for both states. In this case the several curves no longer merge at low x because, although $\theta_{s,x}$ approaches zero, the character of the predominant flexible state is different for each different choice of K_f. Nor do the curves merge at larger x, where for each curve a different flexible form prevails in approximately half the residues of the chain.

It is obviously necessary to investigate the dependence of the calculated $\langle s_x^2\rangle_0/xL^2$ vs. x curves on s and σ. Results of this investigation are given in Figures 5 and 6, where we have chosen K_s = 5.5 kcal/mol, K_f = 3.0 kcal/mol, and ϕ_0,ψ_0 = 0,0° for both states. In Figure 5 the dependence on s of $\langle s_x^2\rangle_0/xL^2$ vs. x is shown for $\sigma = 1.1 \times 10^{-5}$. The

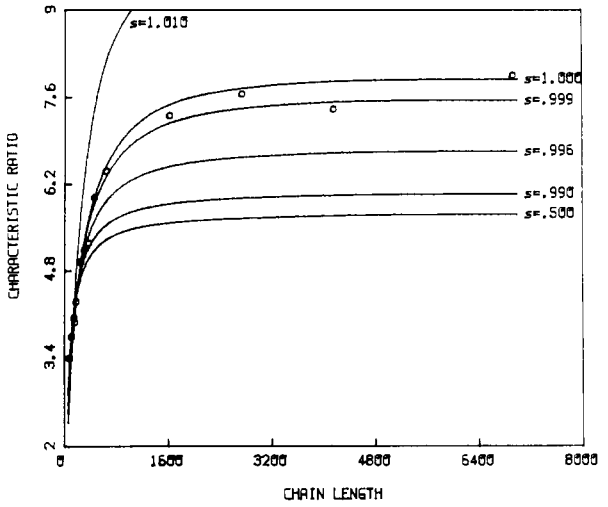

Figure 5. Calculated dependence of $\langle s_x^2\rangle_0/xL^2$ on x for CTC using a two-state model with various values of s and fixed values of all other parameters.

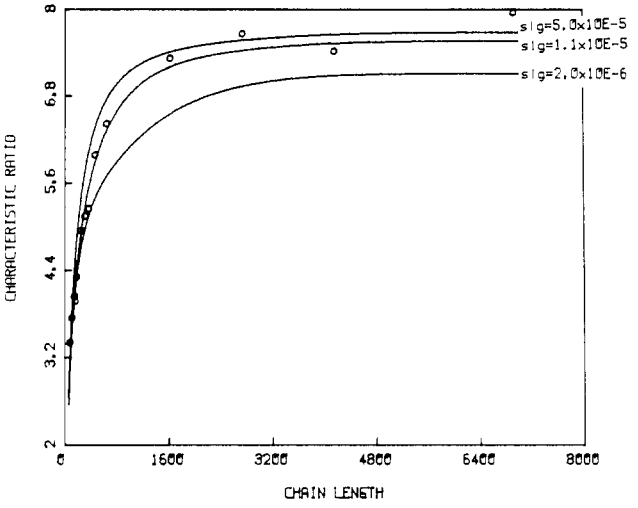

Figure 6. Calculated dependence of $\langle s_x^2\rangle_0/xL^2$ on x for CTC using a two-state model with various values of σ and fixed values of all other parameters.

sensitivity of the curves to s is readily interpreted by reference to Figure 5 of the classic paper of Zimm and Bragg,[12] where $\theta_{s,x}$ is seen to become much more strongly dependent on chain length for $s > 1$ than it is for $s \leq 1$. No reasonable fits to the experimental data could be obtained for s greater than about 1.005, because $\theta_{s,x}$ approached unity very rapidly with increasing x. For $s <$ 0.995, $\theta_{s,x}$ was small for all chain lengths investigated. When s is fixed at 0.999 and σ is varied over a 25-fold range, the results of Figure 6 are obtained; similar results obtain also for s slightly greater than unity. Smaller values of σ yield smaller values of $\langle s_x^2\rangle_0/xL^2$ at all chain lengths investigated. This effect is greatest just in the transition region of x, where the chain undergoes a change in behavior from rodlike ($\langle s_x^2\rangle_0/xL^2$ approximately proportional to x) to Gaussian ($\langle s_x^2\rangle_0/xL^2$ independent of x). Thus, modest adjustment of σ is seen to provide a means for altering the shape of the calculated $\langle s_x^2\rangle_0/xL^2$ vs. x curves in this transition region. The effect of σ on the shape of these curves is readily understood from plots (see Figure 8) of $\theta_{s,x}$ vs. x for various σ, where $\theta_{s,x}$ is found to increase more slowly with x the smaller σ.

Extensive variation of the several parameters of the theoretical calculation led to the "best" fit to the CTC data shown in Figure 7, where K_s = 7.5 kcal/mol, K_f = 4.0

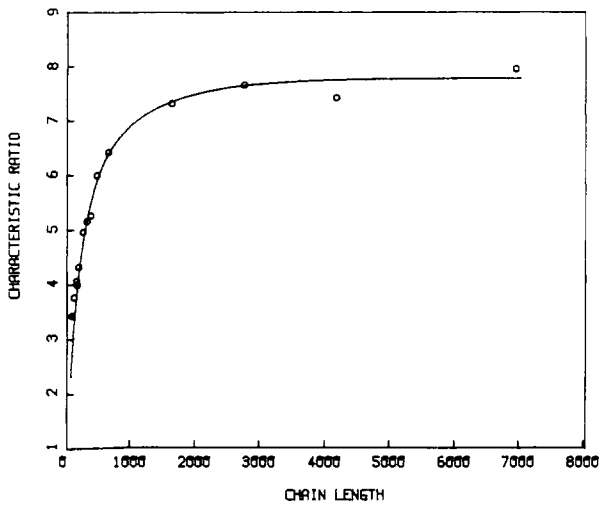

Figure 7. Best theoretical fit to the experimental dependence of $\langle s_x^2\rangle_0/xL^2$ vs. x for CTC using a two-state model with parameters described in the text.

kcal/mol, $\phi_0,\psi_0 = 70,0°$ for both states, $s = 0.9997$, and $\sigma = 1.1 \times 10^{-5}$. Several similar choices of these parameters were also capable of producing fits equally satisfactory. For example, $K_s = 5.5$ kcal/mol, $K_f = 3.0$ kcal/mol, $\phi_0,\psi_0 = 0,0°$ for both states, $s = 0.9995$, and $\sigma = 1.1 \times 10^{-5}$ produced a curve that fit the experimental points at least as well as the curve drawn in Figure 7. Choice of the best fit parameters of Figure 7 was, however, based on the considerations that follow. In an effort to examine the possible influence of the phenylcarbamate substituent groups on the energy surface for a dimeric segment of CTC, additional conformational energy surfaces were calculated with the methods used to produce Figure 1. In these calculations the substituents at O(2), O(3), and O(6) were simulated by structureless spheres of various sizes. These calculations suggested that the presence of bulky substituents at these sites alters the energy surface of Figure 1 so as to shift the conformational domain most free of steric conflicts to the region centered near $\phi,\psi \simeq 70,0°$. For the two-state model leading to the fit shown in Figure 7 we therefore chose $\phi_0,\psi_0 = 70,0°$ for both states. The parameter σ was assigned the value 1.1×10^{-5} extracted from the chain length dependence of the thermal transition in critical dielectric frequency, and s was adjusted to optimize the fit to the $\langle s_x^2\rangle_0/xL^2$ data.

It is evidently of interest to know how well the artificial parabolic potential surfaces of circular cross section approximate the true potential surface for a dimeric segment of CTC. The energy surface in Figure 1, as well as those calculated in efforts to simulate more closely the phenylcarbamate-substituted dimer, is distinctly noncircular, but efforts to approximate this shape more accurately produced no improvement in the fit to the experimental $\langle s_x^2\rangle_0/xL^2$ data while introducing a substantially larger number of adjustable parameters into the calculation. We believe it is best simply to compare the parabolic and more realistic energy surfaces in terms of the conformational freedom that they confer on the chain as measured by the configurational entropy, ΔS_c.[10,27]

This comparison is provided in Table I, where the contribution, ΔS_c, to the entropy of the polymer chain per residue from the conformational variables ϕ,ψ is presented for a variety of potential energy surfaces for the dimeric chain segment. Column 1 of the table gives the dimensions ($\Delta\phi = \Delta\psi$) of square-well energy surfaces having zero energy in a domain of conformation space with dimensions $\Delta\phi \times \Delta\psi$ radians squared and infinite energy elsewhere.

Table I
ΔS_c Free Rotation Equivalents

$\Delta\phi = \Delta\psi$, deg	ΔS_c, cal/(K mol)	K,[a] kcal/mol
10	−6.94	
20	−4.18	
33	−2.19	30
41	−1.36	20
43	−1.10	maltose
47	−0.783	15
57.3	0	
57.5	0.017	10
60	0.162	cellobiose
66	0.560	8
66.4	0.589	7.5
78	1.21	5.5
91	1.84	4
105	2.41	3
360	7.30	

[a] Parabolic steepness parameter.

Column 2 gives the entropy in cal/(deg mol) calculated[10,27] from the square-well potential surfaces. The zero of entropy on this scale is seen to be associated with a square-well energy surface with dimensions of one radian squared. Column 3 lists other energy surfaces employed in the present work. Those labeled 30K, 20K, etc. are parabolic surfaces of circular cross section; the surface labeled cellobiose refers to that shown in Figure 1.

The configurational entropy ΔS_c associated with the cellobiose surface is equivalent to that of a square-well energy surface of square cross section with dimensions $\Delta\phi = \Delta\psi = 60°$. The parabolic 4K and 7.5K surfaces employed in the best fit to the CTC data both display greater conformational freedom, as measured by ΔS_c, than does the cellobiose surface. This seems unrealistic, given the expected effect of the bulky phenylcarbamate substituents. It must, however, be recognized that the cellobiose energy map of Figure 1 leads, using a one-state model, to a calculated asymptotic characteristic ratio $\langle s_x^2\rangle_0/xL^2$ of about 17, which exceeds the observed characteristic ratio of CTC by a factor of more than 2 and bespeaks an unrealistically inflexible cellulosic chain. The tendency of energy surfaces for cellulosic chains, based on seemingly realistic assumptions about skeletal geometry and potential functions, to suggest chains that are unrealistically extended is well-known.[17,28] Cellulosic chains, including CTC with its bulky substituents, are in fact considerably less extended and more flexible than the simple cellobiose energy surface would suggest; the origin of the extra flexibility probably lies in the occurrence of a *small* proportion of glucose ring conformers other than the *C*1 form normally assumed to be present exclusively in cellulosic chains.[10,11,17,27,28]

Since conformational isomerism of the sugar rings is not allowed for in the present model, it is not surprising that dimeric energy surfaces reflecting greater conformational freedom than that for cellobiose with both residues in the *C*1 ring conformation are required to fit the experimental data. In fact the 4K energy surface employed for the flexible state in the best fit to the CTC data, when used in a one-state calculation with $\phi_0,\psi_0 = 70,0°$, yields an asymptotic value of $\langle s_x^2\rangle_0/xL^2 = 5.6$, which is very close to the measured characteristic ratio of cellulose acetate (DS = 2.45).[29] This surface then appears to provide a plausible model for the CTC chain in the flexible state, which is presumed to be free of the long-range interactions postulated to stabilize the stiff state. In the best fit model, when the observed value of $\langle s_x^2\rangle_0/xL^2$ is fit at very long chain length, the model chain incorporates nearly 50% of the residues in the stiff state. Because the interaction stabi-

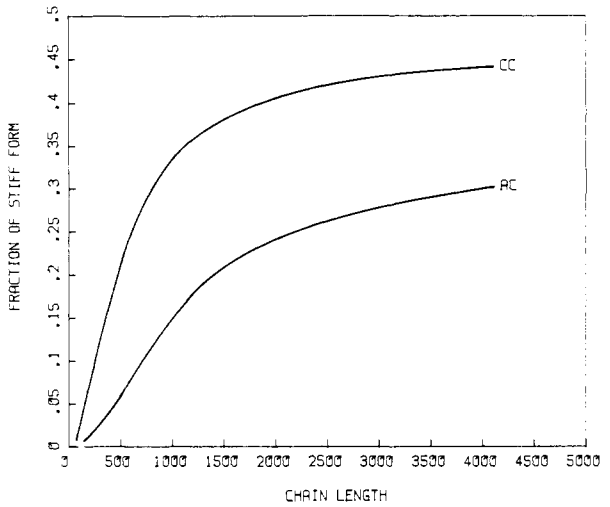

Figure 8. Calculated variation of the fraction of residues in the stiff state $\theta_{s,x}$ as a function of x for the best fit models for CTC ($s = 0.9997$, $\sigma = 1.1 \times 10^{-5}$) and ATC ($s = 0.9992$, $\sigma = 2.0 \times 10^{-6}$).

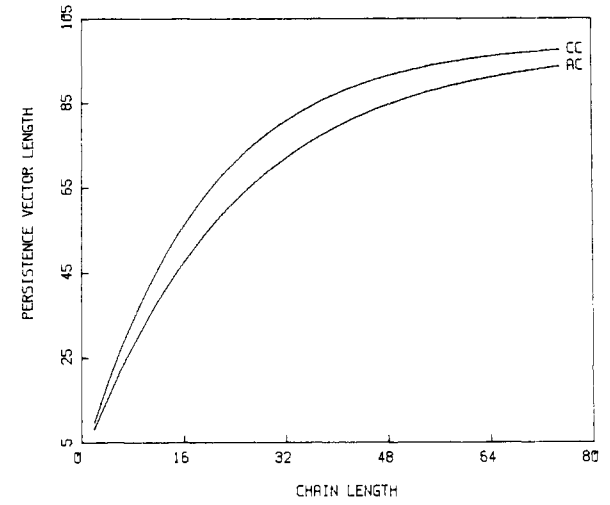

Figure 9. Calculated variation of the persistence length a_x (in Å) as a function of x for the best fit models for CTC and ATC.

lizing this state is postulated to be very cooperative ($\sigma = 1.1 \times 10^{-5}$), residues in the stiff and flexible states occur at high chain length in long sequences averaging $\sigma^{-1/2} \simeq 300$ residues in length.[12] If the model chain were to be converted exclusively to the stiff form, its characteristic ratio would be 10.4, and the chain would still be considerably less extended than the cellulosic chain suggested by the cellobiose map of Figure 1.

It is of interest to observe in Figure 8 the dependence of $\theta_{s,x}$ on x for the best fit model for CTC. The fraction of residues in the stiff state increases rather slowly with chain length and is still about 10% below its high chain length asymptote when $x = 4000$. The length a_x of the persistence vector $\langle r_x \rangle$ is shown as a function of chain length in Figure 9. The persistence length a_x calculated from the model has converged at $x = 200$ to within 97% of its calculated asymptotic value of 110 Å. This asymptotic result is in excellent agreement with experimental determinations[4-7] of the Kratky–Porod persistence length[30] of CTC in dioxane solution. The correlation function f_x, plotted for $2 \leq x \leq 75$ in Figure 10, measures the correlation of virtual bonds 1 and x in a chain of x residues. This quantity, calculable from the model, provides a measure in units of numbers of residues of the directional persistence of the chain and is, hence, a useful adjunct to the persistence length, which measures the persistence in

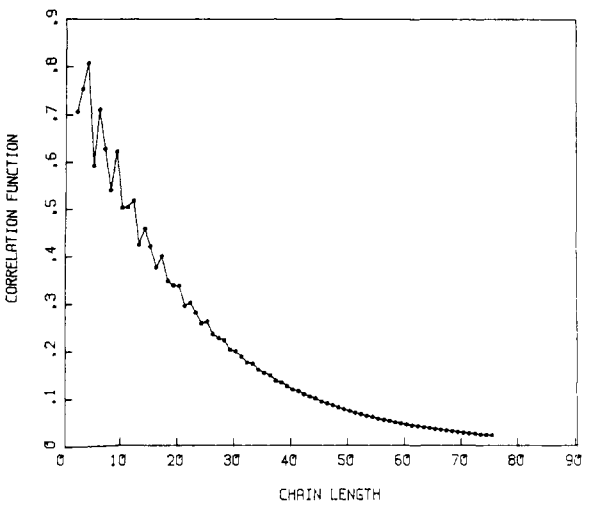

Figure 10. Calculated variation of the end-bond correlation function f_x as a function of x for the best fit model for CTC.

distance units. For CTC f_x remains below e^{-1} for $x \geq 18$; at $x = 75$, f_x has fallen to 0.02, and $f_x = 0.0001$ at $x = 200$. The oscillatory behavior of f_x in the range of small x has a periodicity of 2–3, which reflects the helical character of a cellulosic chain confined to the position $\phi_0,\psi_0 = 70,0°$ in ϕ,ψ conformation space. This feature of Figure 10, which reflects helical persistence, is no longer perceptible for $x > \sim 35$. Reference to Figure 8 will disclose that directional correlations, as measured by either a_x or f_x, have dissipated before the chain is long enough for any substantial fraction of residues to be present in the stiff state. The characteristic ratio of the radius of gyration, however, converges much more slowly with chain length. It continues to change with x throughout the range in which $\theta_{s,x}$ is a function of x and thus serves as a suitable experimental observable to help fix the parameters of the molecular theory. It is also noteworthy that the correlation length measured by the decay of f_x is much smaller than the length of the cooperative unit for long chains, i.e., 300 residues.

Chain Length Dependence of $\langle s_x^2 \rangle_0 / xL^2$ for ATC. A conformational energy diagram for a dimeric segment of unsubstituted amylose is given in Figure 1 of ref 31. The energy minimum, marked with an X in this diagram, corresponds to a residue conformation which, if repeated regularly in sequence, produces a helix with approximately sixfold multiplicity and a relatively small pitch. In order to increase the mean pitch of wormlike pseudohelical chains employed in modeling the behavior of ATC, parabolic potential surfaces were centered at $\phi_0,\psi_0 = -50,-40°$, or approximately halfway between the positions marked X and Y in the conformational energy diagram cited. The resulting increase in mean pitch (1) serves to accommodate the bulky phenylcarbamate substituent groups between turns of the wormlike chains and (2) facilitates reproduction with the model of the large chain extension of ATC using parabolic potential surfaces possessing reasonable conformational freedom.

The convergence of $\langle s_x^2 \rangle_0 / xL^2$ for ATC to its high chain length asymptote is substantially slower than that of CTC as seen in Figure 11, where the calculated curves for various one-state models are shown. In comparison with CTC considerably steeper parabolic potential surfaces are required to fit the asymptotic value of the characteristic ratio. It should be observed that the asymptotic characteristic ratio of ATC exceeds that of CTC only because L^2 is smaller for ATC; at large chain length $\langle s_x^2 \rangle_0 / x$ for CTC exceeds that for ATC by a factor of 1.12. The requirement

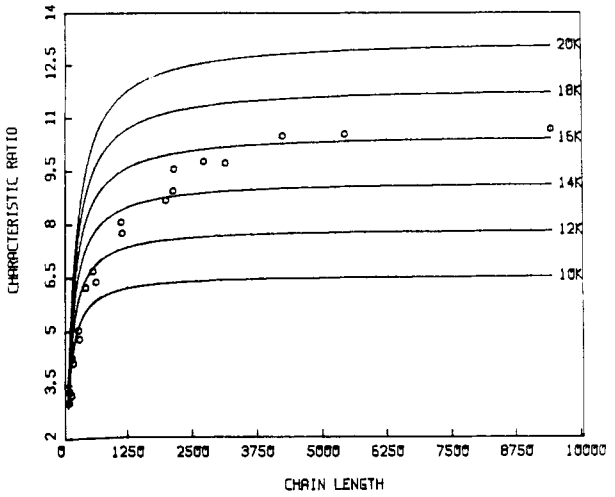

Figure 11. Circles represent experimental results[3] for the characteristic ratio $\langle s_x^2\rangle_0/xL^2$ as a function of degree of polymerization x for ATC. Curves are calculated from a one-state model with various parabolic potential surfaces as described in the text.

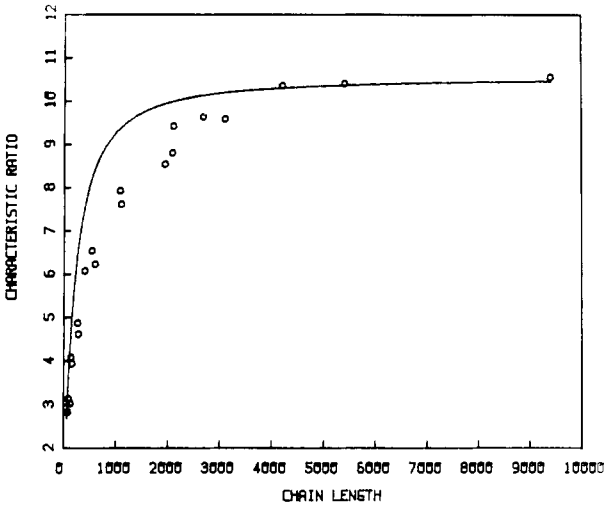

Figure 12. Calculated dependence of $\langle s_x^2\rangle_0/xL^2$ on x for ATC using a two-state model. See text for details.

for steeper and more constrained (see Table I) energy surfaces to fit the asymptotic behavior of the ATC chain arises from the compact pseudohelical trajectory of chains confined to the vicinity of $\phi_0,\psi_0 = -50,-40°$ in conformation space.

No two-state model could be found to fit the chain length dependence of $\langle s_x^2\rangle_0/xL^2$ for ATC in the transition region from rodlike to Gaussian behavior, if the parameter σ was constrained to equal 3.0×10^{-5} as deduced from the observed chain length dependence of the critical dielectric frequency. Attempts to fit the data included trials with a variety of choices for ϕ_0,ψ_0, including the choice $\phi_0,\psi_0 = -20,-170°$, which placed the minimum of the parabolic potential surface at the position of the secondary minimum of the maltose conformational energy map (Figure 1, ref 31) corresponding to the most extended conformations of the amylosic chain. A typical result is shown in Figure 12, in which the curve was computed using $K_s = 16$ kcal/mol, $K_f = 8$ kcal/mol, $\phi_0,\psi_0 = -20,-170°$ for both states, $s = 1.00$, and $\sigma = 3.0 \times 10^{-5}$.

In order to fit the data it was necessary to decrease σ by more than a factor of 10 to 2.0×10^{-6}. With this choice of σ a best fit to the ATC data was achieved with $K_s = 30$ kcal/mol, $K_f = 10$ kcal/mol, $\phi_0,\psi_0 = -50,-40°$ for both states, and $s = 0.9992$. The fit obtained using this model

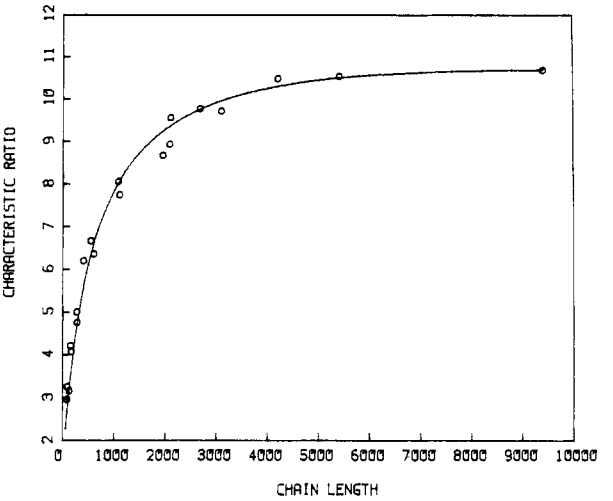

Figure 13. Best theoretical fit to the experimental dependence of $\langle s_x^2\rangle_0/xL^2$ vs. x for ATC using a two-state model with parameters described in the text.

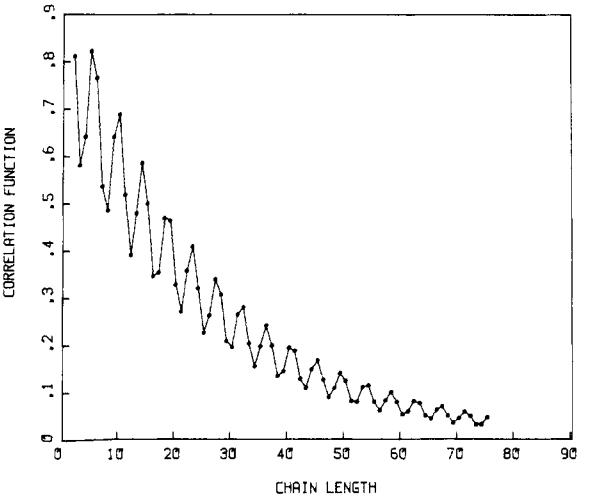

Figure 14. Calculated variation of the end-bond correlation function f_x as a function of x for the best fit model for ATC.

is shown in Figure 13. Reference to Table I shows that the potential surface for the stiff state provides less conformational freedom, as measured by ΔS_c, than the more realistic maltose surface (Figure 1, ref 31), whereas the surface for the flexible state provides more freedom. The experimental value of $\langle s_x^2\rangle_0/xL^2$ for aqueous amylose, and that calculated using a one-state model from the maltose map, is, however, slightly less than unity,[31] whereas the 30K and 10K surfaces yield, respectively, 19 and 6.5. Thus the conformers that predominate near $\phi_0,\psi_0 = -50,-40°$ are much more extended on the average than those of the maltose surface. This circumstance simply reflects the dramatic effect of phenylcarbamate trisubstitution on the amylosic chain conformation, an effect much larger than its counterpart in the cellulosic chain.

The effect of reducing σ to 2.0×10^{-6} is seen clearly in Figure 8 where the fraction of residues in the stiff state is observed to increase much more slowly with x for ATC than is the case for CTC. Figure 9 shows that the calculated persistence length of ATC is somewhat smaller than that of CTC. At infinite chain length a_x achieves an asymptotic value of 103 Å; this can be compared with the value 163 Å reported from experimental observations.[3,7] Directional correlations in ATC, as measured by the correlation function f_x, are found in Figure 14 to dissipate more slowly for ATC than for CTC. Not until $x \geq 24$ does

f_x fall permanently below e^{-1}. The 4–5-fold periodicity in f_x persists beyond $x = 75$, where $f_x = 0.046$; at $x = 200$, $f_x = 0.0003$. The longer range directional correlations implicit in f_x for the ATC model compared to the CTC model are an obvious reflection of the more constrained parabolic energy surfaces required to fit the $\langle s_x^2\rangle_0/xL^2$ vs. x data for ATC. Comparison of the calculated values of a_x and f_x for CTC and ATC shows clearly how these two parameters can provide complementary information about polymer directional correlations.

One other plausible model for ATC was investigated. It is conceivable that the stiff and flexible states of ATC occupy distinctly different regions of the residue conformation space. For example, the long-range interactions of phenylcarbamate substituent groups postulated to stabilize the stiff state may occur only when the substituent group alignment is that which occurs in the fully extended conformations characteristic of the secondary minimum on the maltose energy map. Transition from the flexible to the stiff state with increasing x may then involve a significant change in residue conformation, e.g., from the primary to the secondary minimum. We have, in fact, investigated the opposite situation, taking $\phi_0,\psi_0 = -20,-170°$ for the flexible state and $\phi_0,\psi_0 = -50,-40°$ for the stiff state. The motivation for this choice is that since the stiff state, thus chosen, is also the one characterized by less extended chain conformations, the slow transition of $\langle s_x^2\rangle_0/xL^2$ from rodlike to Gaussian behavior in ATC might be more effectively modeled. With $s = 1.00$ and $\sigma = 3.0 \times 10^{-5}$ and for various choices of K_s and K_f, no adequate fit to the experimental data could be achieved. When the data were fit in the asymptotic region, curves resembling that in Figure 12 were always observed. We have no doubt that the data could be fit with models of this type, provided a small enough value of σ were chosen, but we currently have no justification for this elaboration of the model relative to the model used to produce the best fit shown in Figure 13. It should be observed, however, that the very small σ value required to fit the ATC data might result in part from a large interfacial free energy associated with the junction zones between chain segments in two quite different conformational states.

Acknowledgment. The work reported here has been supported by NSF Grant PCM 79-23041. This work was begun when D.A.B. was a visitor at the Institut für Makromolekulare Chemie, Universität Freiburg, under the sponsorship of the John Simon Guggenheim Memorial Foundation. We also acknowledge the award to B.H. of an ACS Division of Polymer Chemistry Summer Scholarship sponsored by the Proctor and Gamble Co., summer 1980.

References and Notes

(1) Burchard, W. *Z. Phys. Chem. (Frankfurt/Main)* **1964**, *42*, 293.
(2) Burchard, W. *Makromol. Chem.* **1965**, *88*, 11.
(3) Burchard, W. *Br. Polym. J.* **1971**, *3*, 214.
(4) Gupta, A. K.; Marchal, E.; Burchard, W. *Macromolecules* **1975**, *8*, 843.
(5) Noordermeer, J. W. M.; Daryanani, R.; Janeschitz-Kriegl, H. *Polymer* **1975**, *16*, 359.
(6) Gupta, A. K.; Cotton, J. P.; Marchal, E.; Burchard, W.; Benoit, H. *Polymer* **1976**, *17*, 363.
(7) Sutter, W.; Burchard, W. *Makromol. Chem.* **1978**, *179*, 1961.
(8) Gupta, A. K.; Marchal, E.; Burchard, W.; Pfannemueller, B. *Macromolecules* **1979**, *12*, 281.
(9) Arnott, S.; Scott, W. E. *J. Chem. Soc., Perkin Trans. 2* **1972**, 324.
(10) Brant, D. A.; Goebel, K. D. *Macromolecules* **1975**, *8*, 522.
(11) Brant, D. A. *Q. Rev. Biophys.* **1976**, *9*, 527.
(12) Zimm, B. H.; Bragg, J. K. *J. Chem. Phys.* **1959**, *31*, 526.
(13) Poland, D. "Cooperative Equilibria in Physical Biochemistry"; Clarendon Press: Oxford, 1978; Chapter 4.
(14) Hayashi, Y.; Teramoto, A.; Kawahara, K.; Fujita, H. *Biopolymers* **1969**, *8*, 403.
(15) Okita, K.; Teramoto, A.; Fujita, H. *Biopolymers* **1970**, *9*, 717.
(16) Goebel, C. V.; Dimpfl, W. L.; Brant, D. A. *Macromolecules* **1970**, *3*, 644.
(17) Goebel, K. D.; Harvie, C. E.; Brant, D. A. *Appl. Polym. Symp.* **1976**, *28*, 671.
(18) Burton, B. A.; Brant, D. A., submitted.
(19) Jordan, R. C.; Brant, D. A.; Cesàro, A. *Biopolymers* **1978**, *17*, 2617.
(20) Brant, D. A.; Burton, B. A. In "Solution Properties of Polysaccharides"; Brant, D. A., Ed.; American Chemical Society: Washington, D.C., 1981, Chapter 7; ACS Symp. Ser. No. 150.
(21) Cook, R.; Moon, M. *Macromolecules* **1980**, *13*, 1537.
(22) Flory, P. J.; Miller, W. G. *J. Mol. Biol.* **1966**, *15*, 284.
(23) Miller, W. G.; Flory, P. J. *J. Mol. Biol.* **1966**, *15*, 298.
(24) Flory, P. J. *Macromolecules* **1974**, *7*, 381.
(25) Brant, D. A.; Dimpfl, W. L. *Macromolecules* **1970**, *3*, 655.
(26) Flory, P. J. "Statistical Mechanics of Chain Molecules"; Wiley-Interscience: New York, 1969; Chapter 4.
(27) Brant, D. A. In "The Biochemistry of Plants"; Preiss, J., Ed.; Academic Press: New York, 1980; Vol. 3, Chapter 11.
(28) Brant, D. A.; Hsu, B., in preparation.
(29) Tanner, D. W.; Berry, G. C. *J. Polym. Sci., Polym. Phys. Ed.* **1974**, *12*, 941.
(30) Kratky, O.; Porod, G. *Recl. Trav. Chim. Pays-Bas* **1949**, *68*, 1106.
(31) Jordan, R. C.; Brant, D. A. *Macromolecules* **1980**, *13*, 491.

Model Calculation of the Conformational Entropy of the High-Pressure Intermediate Phase of Polyethylene

Richard G. Priest

Naval Research Laboratory, Washington, D.C. 20375. *Received January 19, 1982*

ABSTRACT: A model for the high-pressure intermediate phase of polyethylene is outlined. The focus of the model calculation is on the entropy associated with dihedral angle fluctuations of the polymer chain confined by its neighbors to a cylindrical cavity. The constraint of confinement models the intermolecular interactions. Intramolecular interactions are modeled by a conventional dihedral angle potential. An integral equation version of the transfer matrix method is developed in order to analyze the model. In addition to the calculation of the entropy, the formalism allows a calculation of structural properties of the intermediate phase. The correlation with experimental data is discussed.

I. Introduction

The high-pressure intermediate phase of polyethylene, HPIP, has been the subject of a number of experimental investigations.[1] In contrast to the wealth of data, comparatively few theoretical modeling studies have appeared.[2-4] In an earlier paper,[5] I, an integral equation method for the calculation of the entropy of chains confined to cylinders was developed. Such a model is relevant